

Multiresolution analysis for efficient, high precision all-electron density-functional calculations

Torkel D. Engeness[†] and T.A. Arias[‡]

[†] Department of Physics, Massachusetts Institute of Technology, Cambridge, MA 02139

[‡] Laboratory of Atomic and Solid State Physics, Cornell University, Ithaca, NY 14853

Multiresolution analysis of electronic structure affords the opportunity to capture the full physics of atomic cores in a systematically improvable manner. Applying new techniques, we demonstrate for the first time that multiresolution analysis of all-electron calculations within density-functional theory can be carried out to high precision with a computational effort comparable to that of the corresponding plane-wave pseudopotential calculation, which neither captures the full core physics nor is systematically improvable. With this approach, we present calculations of paramagnetic core-level shifts where local density-functional theory is the sole uncontrolled approximation.

Draft date: February 7, 2020.

I. INTRODUCTION

Over the last several decades, the *ab initio* density-functional approach has proven an accurate, reliable and effective tool for the study of condensed matter. It has found application in such diverse areas as the study of surfaces, point defects, melting, diffusion, plastic deformation, disorder, catalysis, phase transitions and chemical reactions [1]. In principle, the only approximation required in the practice of density-functional theory is some model for exchange and correlation effects. The fact that the forms for exchange and correlation are universal and independent of *a priori* knowledge of the physics or chemistry of the systems under study gives reason for far greater confidence in the predictions of density-functional calculations than those of their semi-empirical counterparts.

Present practice of electronic structure calculation, however, falls short of this ideal. All approaches used in current production employ prior knowledge of chemistry as a criterion for freezing out degrees of freedom in order to deal with the special demands of representing physics near the Coulomb singularity of the atomic nucleus. While such schemes succeed in making *ab initio* studies of complex phenomena accessible, they make it difficult to improve the calculations systematically and face the danger of introducing artificial biases. For instance, Gaussian basis sets are built directly from chemical intuition of how atomic orbitals are expected to polarize [2]. The linear muffin tin orbital (LMTO) method [3], the linearized augmented plane wave (LAPW) method [4], and the full potential LAPW (FLAPW) method [5] all use one type of basis set inside of a set of spheres organized around the nuclei and another type of basis set outside of the spheres, thus treating physics differently in different regions. Finally, the pseudopotential, or "frozen core", approximation, ignores potentially important effects such as core polarization and interferes with the valence wave functions. As a result, it is not uncommon for different groups using different techniques, or

even the same technique, to disagree on the predictions of density-functional theory.

If one could perform *ab initio* calculations with comparable computational effort, but without the biases of the above approaches and with the ability to systematically improve the basis, one finally could access directly the predictions of density-functional theory without ambiguity. Also, one could better explore the development of improved energy functionals, which demands not only better functionals but also the use of basis sets with highly controlled precision sufficient to resolve reliably the associated millihartree-level improvements.

Indeed, wavelet bases do not incorporate any prior knowledge of electron physics and provide a natural framework for systematic expansion of the high spatial frequencies which electrons exhibit near nuclei. Pioneering *all-electron* density-functional calculations based on multiresolution analysis have been reported, first on atoms [6] and then molecules [7,8]. Other applications of multiresolution analysis to related problems include single-electron problems [9], pseudopotential calculations [10–12] and the solution of Poisson's equation [13]. The initial applications to electronic structure, however, were based on relatively primitive techniques and were never demonstrated to produce results at the limits of the accuracy of density-functional theory nor to provide results with an efficiency comparable to standard techniques such as the pseudopotential plane-wave approach. We believe that the reason for this shortcoming is that standard approaches in the wavelet literature are designed for applications, such as digital signal processing, which have far different demands than do continuum problems in the physical sciences. In response, we have taken a different tact. Starting with the fundamental principle underlying wavelet theory, multiresolution analysis [14–16], we have developed a unique set of methods and tools designed specifically for the treatment of continuum problems [6,7,17]. Below, we report the results of the use of these new techniques.

II. CHOICE OF BASES

Figure 1 illustrates the general structure of the multiresolution analyses employed in this work. These begin with a coarse representation consisting of a uniform orthorhombic grid of rather extended basis functions (large circles in the figure) placed in a unit cell with periodic boundary conditions (dashed square). Additional basis functions of intermediate extent (medium circles) on a grid of one-half the original spacing then carry details which the coarse representation does not. Yet smaller functions (small circles) on a grid of one-half the spacing of the intermediate grid carry information for one further scale down. Repetition of this construction provides for any desired level of resolution.

With appropriate choice of basis functions, multiresolution analysis ensures the crucial result which allows the following calculations to achieve systematic convergence, that such a multiscale basis spans exactly the same function space as would a uniform basis of functions on the finest scale. The basic idea is to insist that each basis function be expressible *exactly* as a linear combination of translates of itself scaled down by a factor of two,

$$b(\vec{x}) = \sum_{\vec{n}} c_{\vec{n}} b(2\vec{x} - \vec{n}), \quad (1)$$

where $b(\vec{x})$ is the basis function and \vec{n} ranges over all triplets of integers. The above equation is known as the *two-scale* relation. Applied recursively, this relation implies that all coarser functions in the basis are expressible exactly as linear combinations of functions on the finest scale and, therefore, that the multiscale basis is equivalent to the basis on the finest scale. For a full review, see [7].

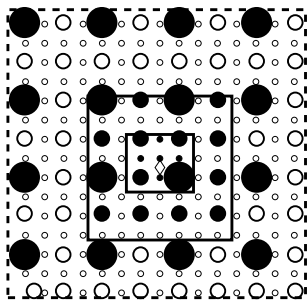


FIG. 1. Schematic representation of a two-dimensional restricted multiresolution analysis of three levels of resolution. (See text for description.)

The basis consisting of *all* functions indicated in the figure contains precisely as many functions as the equivalent uniform basis on the finest scale. Thus, its direct use would represent no savings. However, the coefficients of the basis functions on the finest levels of the multiresolution basis represent high frequency details and hence are significant only in the vicinity of the nucleus (diamond in the figure). Consequently, the finest scale functions are

necessary only in the region closest to the nucleus (small solid square), and the intermediate scale functions are necessary only in a region extending somewhat further from the nucleus (medium solid square). *Restricting* the multiresolution analysis by maintaining only those functions (filled circles) within the *refinement regions* for each scale affords significant savings while affecting the final results negligibly — shortly below in Section III C, we demonstrate the effects of such restriction to be controllable down to at least the *microhartree* per atom level.

To describe fully the bases used in our calculations, we must specify both the original multiresolution analysis and its restriction. All multiresolution analyses employed in this work begin with a coarsest level of one bohr spacing and employ basis functions of the “third-order *semicardinal* type”. This means that the functions satisfy the two-scale relation (1) with the two additional constraints of “cardinality,”

$$b(\vec{n}) \equiv \delta_{\vec{n},\vec{0}} \quad (2)$$

(zero value on all integer points but $\vec{n} = \vec{0}$), and “exact reconstruction” of multinomials up to third order,

$$x^\alpha y^\beta z^\gamma \equiv \sum_{\vec{n}} n_x^\alpha n_y^\beta n_z^\gamma b(\vec{x} - \vec{n}); \quad 0 \leq \alpha, \beta, \gamma, \leq 3. \quad (3)$$

These two additional constraints, respectively, simplify the computational algorithms considerably and allow third-order interpolative representation of functions such as the electron density. See [7] for a full discussion.

To describe the restrictions employed in this work, we note that they consist of orthorhombic refinement regions. Thus, specification of the restriction reduces to identification of the dimension (N_x, N_y, N_z) and location of these regions at each *level* of resolution. Because the refinement regions of a finer level (higher level number) are always contained within the refinement region of the next higher level, it is most convenient to identify the location of a refinement region in terms of the displacement of its origin from the origin of its *parent* region in units of the parent’s spacing ($\Delta_x, \Delta_y, \Delta_z$). Using this approach, for example, Table I specifies the two-dimensional restriction which Figure 1 illustrates.

In some cases, such as the restriction for the calculation of the oxygen molecule in Table IV, a single refinement region contains multiple *children*, regions of the next level of refinement. In such cases, we first list the first child with all of its progeny directly underneath and then proceed to the remaining children of the original parent. Ordered and listed with the data as appear in these tables, such a specification is sufficiently general, complete and compact that we use it directly as an input data structure when specifying multiresolution analyses to our software.

III. EFFICACY OF MULTIREOLUTION ANALYSIS OF ELECTRONIC STRUCTURE

A. Kohn-Sham equations in a multiresolution basis

For a full review of the form and solution of the Kohn-Sham equations in a multiresolution basis, see [7]. Here, we sketch briefly the key equations which we use to produce the results in this work. The central quantity in density-functional theory is the energy expressed in terms of the expansion coefficients $C_{\alpha i}$ of the Kohn-Sham orbitals,

$$\psi_i(\vec{x}) = \sum_{\alpha} C_{\alpha i} b_{\alpha}(\vec{x}), \quad (4)$$

where i runs over the Kohn-Sham orbitals and α ranges over the functions in the basis employed in the calculation. In [7,18], we give the appropriate expression for this energy function in an arbitrary basis. This expression involves standard matrix operations, such as the trace Tr , and the basis-dependent matrices

$$\begin{aligned} \mathcal{O}_{\alpha\beta} &\equiv \int b_{\alpha}(\vec{x})^* b_{\beta}(\vec{x}) d^3x \\ L_{\alpha\beta} &\equiv \int b_{\alpha}(\vec{x})^* \nabla^2 b_{\beta}(\vec{x}) d^3x \\ \mathcal{I}_{p\alpha} &\equiv b_{\alpha}(p), \end{aligned} \quad (5)$$

where α and β range over all functions in the basis and p ranges over a set of sample points in real space, which in the present case are the centers of the wavelet basis functions (filled circles in Figure 1). The first two matrices give the overlap integrals and matrix elements of the Laplacian, respectively. The final matrix consists of the values of each basis function at each sample grid point p so that the product of \mathcal{I} with a vector of expansion coefficients transforms it to a vector of values in real space.

In terms of the above matrices, the density-functional expression for the total energy in terms of the expansion coefficients gathered into the matrix C is

$$\begin{aligned} E_{LDA}(C) &= \text{Tr} \left(f C^{\dagger} \left(-\frac{1}{2} L \right) C \right) + (\mathcal{I}^{-1} n)^{\dagger} \mathcal{O} v \\ &+ (\mathcal{I}^{-1} n)^{\dagger} \mathcal{O} \mathcal{I}^{-1} \epsilon_{xc}(n) + \frac{1}{2} [(\mathcal{I}^{-1} n)^{\dagger} \mathcal{O} d], \end{aligned} \quad (6)$$

Here, f is the occupancy of each orbital (typically 2), v is the vector of expansion coefficients of the ionic potential,

$$V_{ion} = \sum_{\alpha} v_{\alpha} b_{\alpha}(\vec{x}),$$

$\epsilon_{xc}(n)$ is the usual exchange-correlation energy of a homogeneous electron of uniform density n , and n and d , respectively, are the electron density evaluated at the sample points and the expansion coefficients of the Hartree potential,

$$n = \text{diag} \left((\mathcal{I} C) f (\mathcal{I} C)^{\dagger} \right) \quad (7)$$

$$d = -4\pi L^{-1} \mathcal{O} \mathcal{I}^{-1} n, \quad (8)$$

where “diag” is the operation of forming a vector from the diagonal elements of a matrix. The final quantity needed to solve the Kohn-Sham equations is the derivative of E_{LDA} with respect to the orbital coefficients C ,

$$\begin{aligned} \frac{\partial E_{LDA}}{\partial C} &\equiv -\frac{1}{2} L C + \mathcal{I}^{\dagger} \text{Diag} \{ \\ &\mathcal{I}^{-\dagger} \mathcal{O} \mathcal{I}^{-1} \epsilon_{xc}(n) + (\text{Diag} \epsilon'_{xc}(n)) \mathcal{I}^{-\dagger} \mathcal{O} \mathcal{I}^{-1} n \\ &+ \mathcal{I}^{-\dagger} \mathcal{O} v + (\mathcal{I}^{-\dagger} \mathcal{O} d) \} \mathcal{I} C, \end{aligned} \quad (9)$$

where $\text{Diag} a$ represents formation of a diagonal matrix with diagonal elements given by the components of the vector a .

To aid the reader’s interpretation of (6-9), we note that these expressions are fully general and applicable not only to wavelets but also to plane waves. These expressions, therefore, represent minor generalizations of the same sequence of operations found typically in plane-wave density-functional codes. For instance, in the computation of the real-space electron density (7), the quantity $(\mathcal{I} C)$ represents the fast Fourier transformation of the orbitals from coefficient to real space, the outer-product $(\mathcal{I} C) f (\mathcal{I} C)^{\dagger}$ is then the real-space density matrix, whose diagonal elements ultimately give the real-space electron density n .¹ Similarly, to find the Hartree potential (8), one first multiplies $\mathcal{I}^{-1} n$ (inverse Fourier transforming the real-space density to coefficient space in the plane wave case), multiplies by \mathcal{O} (for plane waves, a simple volume normalization factor) and then by -4π times the inverse of the Laplacian matrix ($4\pi/G^2$ for plane waves). The terms in Eqs. (6,9) each have similar interpretations.

To produce the results reported below, we minimized the expression (6) over all possible coefficients C , using the diagonally preconditioned conjugate-gradient algorithm augmented with the analytically continued functional approach [19] to handle the orthonormality constraints on the orbitals. Combined with (5-9), this describes our calculations fully and explicitly.

None of the calculations below employ gradient corrected density functionals. During the preparation of the manuscript, however, we were asked to comment on how one would handle the numerical issues which such functionals raise. Our general approach to numerical issues is to note that so long as the evaluation of a given term

¹Eq. (7) is a formal expression. Anticipating the diag operator, practical software computes only the diagonal elements and not the full density-matrix. Similarly, in Eq. (9), rather than forming large matrices such as $\text{Diag} a$ explicitly, our software computes products such as $(\text{Diag} a)b$ by multiplying each element of b by the corresponding element of a .

in E_{LDA} is exact for any finite expansion of the Kohn-Sham orbitals (4), then all numerical issues reduce to the quality of the expansion for the wave functions, which we show below to be well-controlled in multiresolution bases.

Therefore, to avoid numerical instabilities associated with finite differencing to evaluate quantities such as $\nabla n(\vec{x})$, we would evaluate the exact, analytic gradient of the charge density associated with the orbital expansion (4). To do this, we define an additional matrix

$$\mathcal{G}_{p\alpha} \equiv \nabla b_{\alpha}(p),$$

where α and p range as in the definitions (5). The values of $\nabla\psi_i(\vec{x})$ at the sample points p are then

$$\nabla\psi_i(p) = [\mathcal{G}C]_{pi},$$

so that the gradient of the charge density at these points is *exactly*

$$\begin{aligned} \nabla n(p) &= f \sum_i (\nabla\psi_i(p)^* \psi_i(p) + \psi_i(p)^* \nabla\psi_i(p)) \\ &= \sum_i \left([\mathcal{G}C]_{pi}^* f [\mathcal{I}C]_{pi} + [\mathcal{I}C]_{pi}^* f [\mathcal{G}C]_{pi} \right) \\ &= [(\mathcal{I}C)f(\mathcal{G}C)^\dagger + (\mathcal{G}C)f(\mathcal{I}C)^\dagger]_{pp} \\ &\Rightarrow \end{aligned}$$

$$\nabla n = \text{diag} \left((\mathcal{I}C)^\dagger f(\mathcal{G}C) + (\mathcal{G}C)^\dagger f(\mathcal{I}C) \right).$$

When the exchange-correlation function is evaluated using this quantity and inverse-transformed with \mathcal{I}^{-1} , the resulting coefficients, as per the discussion in Section IV, will be exactly the same as would be obtained were the numerical evaluation carried out in a full multiresolution analysis at arbitrary resolution without restriction, thereby mitigating any numerical issues associated with the evaluation of gradient corrected functionals on wave functions expanded as in (4).

B. Systematic convergence

Present feasible approaches to all-electron calculations complicate access to the full predictive power of density-functional theory and the development of new functionals because these methods approach the atomic cores and the valence regions in fundamentally different ways and therefore are difficult to bring to convergence in a systematic manner. While it has been clear for some time that the ability of multiresolution analysis to focus resolution in small regions of space can be exploited to perform all-electron calculations [6–8], the highly systematic nature of multiresolution analysis and the consequent advantages have yet to be explored in the context of electronic structure. We now present the first demonstration of a multiresolution analysis reproducing all-electron

density-functional results with highly systematic convergence down to millihartree accuracy.

For this demonstration, we compare results for atoms as calculated within the local-density approximation as parameterized in [20] using both standard techniques and our multiresolution approach. Atoms provide a convenient test bed because spherical symmetry produces an effective one-dimensional problem which standard techniques then readily solve to a precision controllable to better than 1 nanohartree. To provide a fair measure of how we expect the multiresolution method to perform in practice, all calculations with multiresolution analyses in this work are fully three-dimensional and without any simplifications.

To underscore that our approach is feasible beyond first and second row elements, we have chosen calcium for comparison. To represent the charge distribution of the calcium nucleus (and all nuclei in this work), we use the linear combination of three Gaussian distributions with the widths and charge contents appearing in Table II. This charge distribution reproduces the atomic electron eigenvalues to within 0.5 mH [21], an accuracy which is systematically improvable through a renormalization approach [22]. All calculations and comparisons below are made for this form of nuclear charge distribution. As described above, the multiresolution analysis begins with a spacing of 1 bohr on level zero. To explore the convergence toward the final solution, we perform self-consistent calculations with from seven to nine levels of refinement, for a resolution of down to $1/2^9 \sim 0.002$ bohr. Table III summarizes the restrictions employed for the calculation.

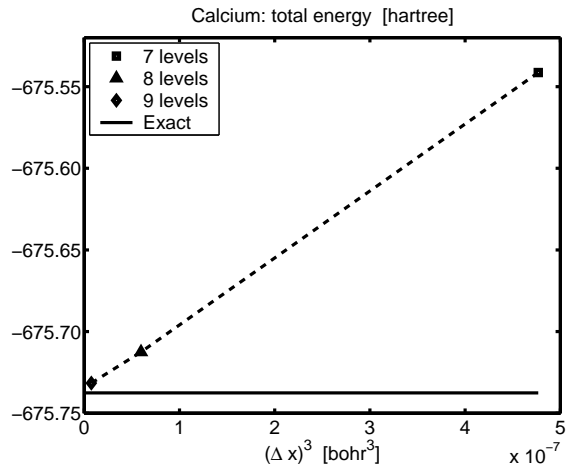


FIG. 2. Error in total all-electron energy within the local density approximation, ΔE , of a multiresolution calculation of an isolated calcium atom at 7, 8 and 9 levels of resolution (squares) below a top level of 1 bohr spacing. The horizontal axis gives the cube of the resolution on the finest scale $(\Delta x)^3$.

Figure 2 shows, as a function of the *cube* of the spacing on the finest level, the difference between the total energy calculated with the multiresolution analysis and the

highly precise solution of the equivalent one-dimensional problem. When we employ nine levels of refinement, the absolute error is 6 mH, one part in 10^5 of the total energy.

The simple, linear approach of the error toward zero in this plot is a direct consequence of the fundamental nature of the basis. The multiresolution analysis which we employ satisfies the two-scale relation and, thus, is equivalent to a uniform basis on the finest scale of resolution *by construction*. The linear behavior evident in the figure, therefore, can be understood *a priori* as a direct consequence of the third-order nature of the semicardinal basis. The only other method which provides this level of analytic understanding of the errors as a function of the size of the calculation is the plane-wave approach. However, large scale plane-wave calculations are only feasible in practice with pseudopotentials and therefore do not systematically converge to the correct all-electron result. Multiresolution analysis, therefore, is unique among *feasible* all-electron approaches in allowing for a high degree of *a priori* understanding of and systematic control over errors.

C. Uniformity of description of space

Present methods demonstrated to be viable for all-electron calculations all treat space near the atomic nuclei differently from the interatomic regions. This inherently biases the description toward the location of the atoms and complicates the evaluation of forces on the atoms [23]. Surprisingly, even under restriction, this effect is nearly absent in multiresolution analysis because of the unique way in which multiresolution analysis represents information.

In direct contrast to the expansion coefficients in finite-element bases or finite-difference calculations, which are in proportion to the *value* of the represented function in the corresponding region of space, the expansion coefficients of the finer-scale functions in a multiresolution analysis represent only the higher-frequency *details* in the corresponding region. The expansion coefficients of the finer-scale functions which are restricted from a multiresolution basis (empty circles in Figure 1), unlike the coefficients which would appear in those regions in traditional approaches, therefore can be made to vanish controllably by expanding the corresponding refinement regions (squares in Figure 1) outward from the nuclei. As the coefficients dropped from the expansion vanish, the restricted multiresolution analysis becomes indistinguishable from the full analysis, and the underlying description of space therefore becomes uniform.

To demonstrate this, we consider the calculation of the total energy of a single atom (aluminum) at different locations in space. For these calculations, we employ a cubic cell of dimension 48 bohr with seven levels of refinement, each consisting of a cubic array of 48^3 basis functions. We begin with the atom centered on a basis

function from the coarsest scale and then move the atom along a coordinate axis in increments so that the nucleus falls directly on the centers of basis functions, eventually sampling functions from each of the eight levels in the calculation. As the atom moves, we add or remove functions from the basis to maintain the atom at the center of each refinement grid while conserving the number of basis functions on each level.

Figure 3 shows the results of the above calculations. Despite the switching on and off of the basis functions and the radically changing nature of the basis function on which the nucleus falls (ranging by over two orders of magnitude in length scale), the root-mean-square fluctuation in the energy is less than 3 *microhartree*, which we could reduce yet further by expanding the extent of the refinement regions. In terms of Pulay-force corrections [23], the maximum fluctuation in energy as we move the atom by $1/64$ bohr (the smallest step for which the basis actually changes) is $2.0\mu\text{H}$, corresponding to a maximum average Pulay force of $\sim 128 \mu\text{H}/\text{B} \approx 0.007 \text{ eV}/\text{\AA}$. This remarkable result makes the multiresolution approach an extremely attractive tool in calculations where the atoms move, such as structural relaxation or molecular dynamics.

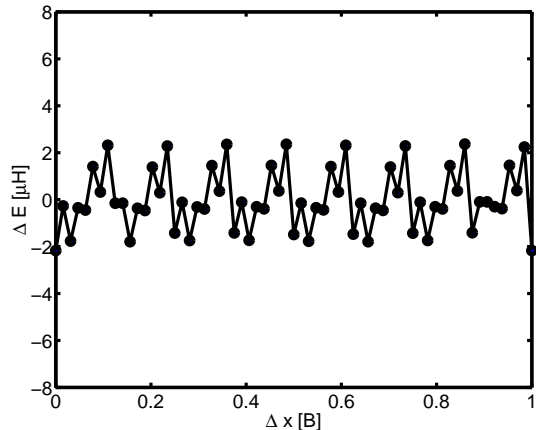


FIG. 3. Fluctuation (ΔE) in total all-electron energy of an isolated aluminum atom as a function of distance (Δx) of the nucleus from the center of a basis function on the coarsest scale. Note that vertical scale is in *microhartree*.

D. Description of chemical bonding

To investigate the efficacy of the multiresolution approach in the description of chemical bonding, we consider the oxygen molecule. Given the paramagnetic nature of this molecule, we carry out the calculation within the local spin-density approximation (LSDA) as parameterized in [24]. To ensure sufficient isolation of the molecule from its periodic images, we employ a supercell of dimensions $14.8\text{\AA} \times 12.7\text{\AA} \times 12.7\text{\AA}$. We then orient the molecule along the long axis of the cell, place the

nuclei at their experimental separation, and employ the multiresolution analysis in Table IV.

For comparison, we also performed, within the same geometry and parameterization of the local spin-density functional, a plane-wave calculation within a periodic supercell of identical dimensions using a pseudopotential optimized for convergence according to the procedure of Rappe *et al.* [25]. This pseudopotential required a plane wave cut-off of 35 hartree to converge the total pseudo-energy to within 0.10 hartree. Given this level of convergence in the total energy and the fact that the fractional error in the variational total energy scales like the square of the fractional errors in non-variational quantities such as the eigenvalues, we estimate the individual eigen-energies to be converged to within about 0.03 hartree at this plane-wave cut off.

Figure 4 compares the Kohn-Sham eigenvalues from the pseudopotential calculation with those from multiresolution analysis. Within the expected convergence of the pseudopotential calculation, the agreement is complete. These results illustrate that the multiresolution approach gives a description of bonding at least as reliable as the standard pseudopotential approach. Because the issue of transferability remains an open question in pseudopotential theory, this result also lends greater credence to the pseudopotential which we have constructed for these calculations. We envisage the use of multiresolution analysis in this way to aide in the construction of pseudopotentials with greater transferability.

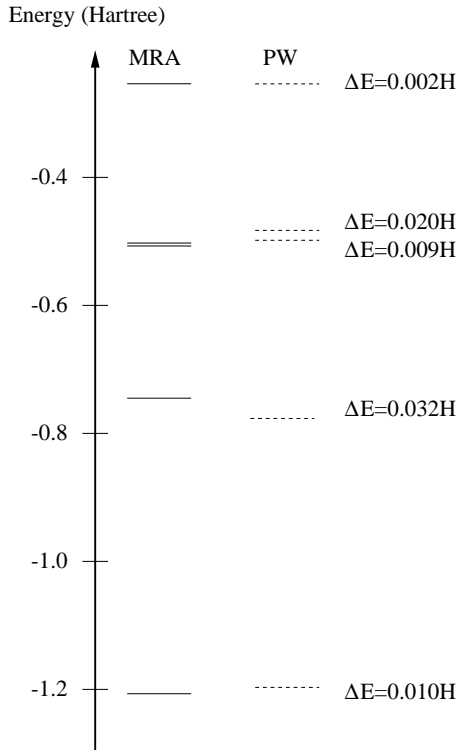


FIG. 4. Kohn-Sham eigenvalues for valence states of the oxygen molecule: results of all-electron multiresolution analysis calculation (MRA) and plane-wave pseudopotential calculation (PW).

IV. COMPUTATIONAL EFFICACY

The computational demands of wavelet-based all-electron calculations in previous works were so extreme that the literature has yet to explore the practicality of the computations. The calculations presented in this work are the first to apply a series of new techniques [7,17,26] to achieve high performance in all-electron problems, placing us in a position to account in detail for the computational effort that our calculations demand and thereby provide a standard against which the performance of future wavelet calculations can be compared. We find that our new techniques make the demands of all-electron calculations sufficiently comparable to those of frozen-core pseudopotential calculations of the same precision to make wavelet calculations a practical alternative.

Rather than using techniques developed for other classes of application, the techniques which we use here are tailored to the specific demands of continuum problems in the physical sciences. Our basis, for instance, technically is not a wavelet basis because its dual consists of sets of Dirac-delta functions. These delta functions, however, are precisely what are needed to recover *exact* representations from samples of physical fields at extremely limited numbers of points in real space [17]. In the present context, this means that the operations \mathcal{I}^{-1} appearing in (6,8,9) always yield precisely the same results as would be obtained were the calculation carried out with a full, *unrestricted* multiresolution analysis of *arbitrary* resolution. (See [7,17].) As evident in (6,8,9), such operations are key in the effective treatment of non-linear couplings such as exchange and correlation effects and evaluation of the Hartree potential. Without this profound result, accurate evaluation of such effects requires evaluation of quantities at a much larger set of points in real space, thereby slowing the calculation considerably. To go along with these new methods for the transforms (\mathcal{I} , \mathcal{I}^{-1} and related operations), we have also developed a class of $O(N)$ methods for multiplication by the operators \mathcal{O} and L with similar exactness properties [7,17]. Finally, to further improve the performance of the calculations, we have developed special cache-optimized algorithms for all of these methods [26].

As a case study, we consider in detail the computational demands of the calculations of the electronic structure of the oxygen molecule presented in Section III D above. To make the comparison with a pseudopotential calculation meaningful, we choose a restriction of the multiresolution analysis (Table IV) and a plane-wave cut off (35 H) which achieve similar convergence in the total energy: 0.08 H and 0.10 H, respectively.

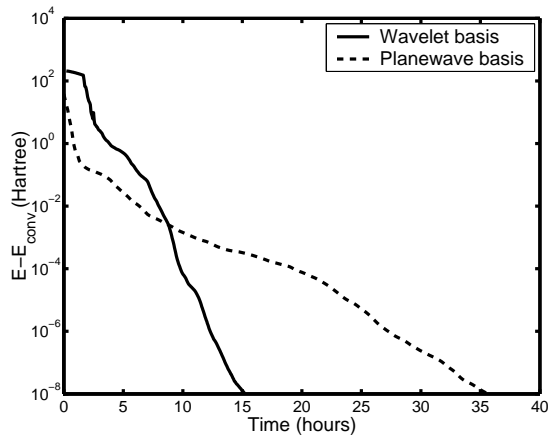


FIG. 5. Convergence of total energy of the oxygen molecule as a function of actual wall-clock time on a 400 MHz Pentium II PC for basis sets reaching a similar level of convergence: plane-wave pseudopotential calculation (dashed curve), all-electron multiresolution analysis calculation (solid curve).

Figure 5 presents the convergence of the total energy as a function of actual wall-clock time on a 400 MHz Pentium II PC both for our wavelet calculation and for a plane-wave pseudopotential calculation performed with the highly optimized DFT++ code [18]. Despite the fact that the pseudopotential calculation freezes out the physics of the core, the absolute convergence for the pseudopotential calculation is slower than that of the all-electron wavelet calculation. These results are the first to establish multiresolution analysis as a *computationally viable*, unbiased and systematic approach to the calculation of all-electron systems.

Several advances have taken place to make possible this favorable comparison. To place these in context, we consider the time required for the single most time consuming *basis dependent* operation in the two calculations, the Laplacian for the wavelet case and the Fourier transform for the plane-wave case. In general, the total time required to perform such operations is

$$T = N_A \frac{N_B N_{F/B}}{N_{F/T}}, \quad (10)$$

where N_A is the number of times the corresponding operation is performed while reaching the desired level of convergence, N_B is the number of functions in the basis, $N_{F/B}$ is the number of floating point operations needed to process each basis function during the operation, and $N_{F/T}$ is the number of floating point operations which the algorithm for the operation achieves per unit time.

Table VI presents these quantities for calculations which achieved the convergence of 10^{-8} H in Figure 5. The table confirms the finding established in earlier works that the total number of basis functions N_B required for both calculations is similar [6,7].

The new algorithms which we employ [7,17] exploit the local nature of the multiresolution basis to produce

a data flow pattern which now is sufficiently simple to reduce $N_{F/B}$ from that of our previous calculations [6] by several orders of magnitude. To multiply by \mathcal{I} , for instance, we apply the two-scale relation (1) recursively until we reach an expansion in terms of functions on the finest scale, which, by virtue of (2), gives the values of the function at each point p . Eq. (1) implies that each step in this recursion is simply a three-dimensional convolution by the sequence $c_{\vec{n}}$. Reference [7] presents methods for wavelet bases which similarly decompose multiplication by all remaining basis dependent matrices (\mathcal{O} , L , \mathcal{I}^{-1} , \mathcal{I}^\dagger , $\mathcal{I}^{-\dagger}$) into three-dimensional convolutions for wavelet bases. For our choice of basis, these convolutions are short and separable, leading to an operation count with a significant advantage over that of the fast Fourier transform: $N_{F/B} \approx 250$ versus $N_{F/B} \approx 75 \log_2(15N)$ (including appropriate factors for mapping the plane-wave sphere into the Fourier transform box). Table VI shows that for the present calculations, the wavelet $N_{F/B}$ is superior by a factor greater than six.

The simpler communication pattern of separable three-dimensional convolutions also allows us to develop special algorithms with significantly improved cache performance and thus processing rates $N_{F/T}$ nearly an order of magnitude improved over that achieved in previously reported wavelet-based electronic structure calculations. Table VI shows that, in fact, we now can achieve floating point operation rates $N_{F/T}$ somewhat superior to those of the highly tuned FFTW Fourier transform package [27], which we employ in the plane wave calculations. Finally, we note as a possible area for future research that the only area where the plane wave calculation holds a significant advantage is in the number of applications required of the rate limiting operator N_A .

The result of all of the above factors is that the plane wave and wavelet calculations require comparable (within a factor of three) amounts of time T in their most time consuming basis-dependent operators. The remaining components of the calculations do consume significant amounts of time and so the total run times (Figure 5) are significantly longer. In the wavelet case, our data for the Laplacian operator accounts for about one-half of the total run time. The additional operations in the plane wave calculations consume a much more significant fraction of the total time. As a result, in this particular case it turns out that the final total run time for the pseudopotential calculation, which does not include the physics of the core explicitly, is in fact noticeably longer than that for the corresponding wavelet calculation.

V. CORE-LEVEL PHYSICS

One great advantage of multiresolution all-electron calculations over their pseudopotential counterparts is the direct access which they give to the full physics of the atomic cores in an unbiased representation. A promising

area of application for such calculations is their use as an aid to the interpretation of experimental techniques which measure environmentally dependent shifts in the core states, such as electron energy loss spectroscopy (EELS) [28] and electron spectroscopy for chemical analysis (ESCA) [29]. As a simple demonstration of the physics accessible through this approach, we consider the environmental dependence of the oxygen $1s$ state in the water and the diatomic oxygen molecules.

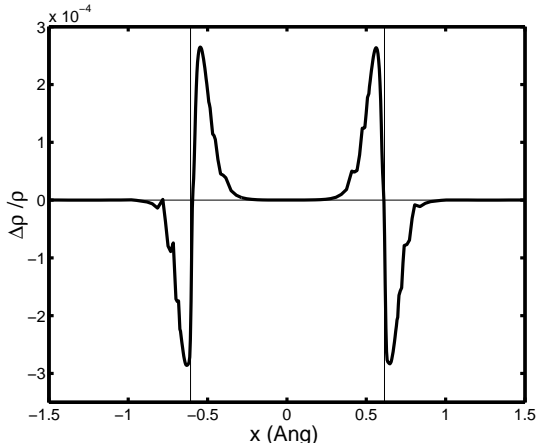


FIG. 6. Difference, along the symmetry axis of the molecule, in total charge density of the oxygen $1s$ states (both spin channels) in going from atomic oxygen to the oxygen molecule. Values expressed as fractions of the peak density of the $1s$ state in atomic oxygen. Vertical lines indicate locations of the oxygen nuclei.

For diatomic oxygen, which is paramagnetic, we use the results of the local spin-density calculations described above in Section III D. For the water molecule and the reference atomic states, we employ the local density approximation as parameterized in [20]. For all calculations, we place the nuclei at their experimentally known locations and employ the multiresolution analyses which Tables IV and V summarize. The general, simple structure of multiresolution analysis allows this brief description to specify the calculations completely.

Our results for the deformation of the $1s$ state of oxygen in the above molecules appear in Figures 6 and 7. Figure 6 shows the change in the total electron density in the oxygen $1s$ states (sum both over spin channels and over bonding and anti-bonding states) in going from atomic oxygen to the oxygen molecule. Despite being quite small (at the 0.03 % level), the core polarization effect is quite clearly defined in our multiresolution analysis, which we emphasize builds no *a priori* knowledge of this polarization into the calculation. Interestingly, we find that, despite the buildup of repulsive valence charge in the bond between the oxygen atoms, the decreased screening of the nuclei is sufficient to produce local electric fields which polarize the core electrons *toward* the center of the molecule.

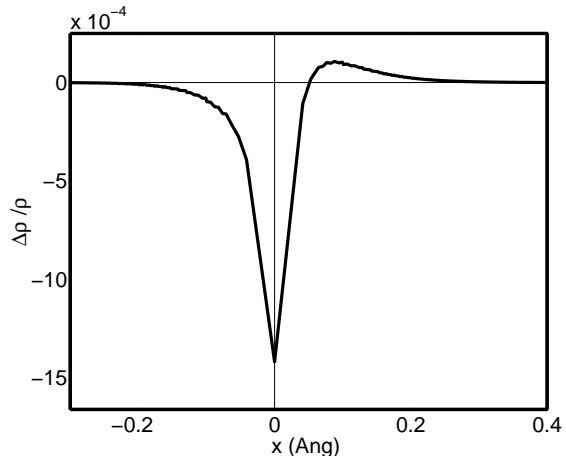


FIG. 7. Difference in charge density of the oxygen $1s$ state in going from atomic oxygen to the water molecule along a line directly toward one of the protons. Values expressed as fractions of the peak density of the $1s$ state in atomic oxygen. Vertical line indicates the location of the oxygen nucleus.

Figure 7 shows the change in the electron density of the oxygen $1s$ state in going from the oxygen atom to the water molecule. Again, the deformation of the $1s$ states is quite clearly described in our multiresolution analysis despite being relatively small (0.16%, somewhat larger than in the oxygen molecule). In the water molecule, the electrons associated with the hydrogen atoms are stripped away and distributed in an approximately spherical shell of charge around the oxygen atom. Similarly to the water molecule, our calculation finds that this lessens the shielding of the protons and leads to the net attraction of the oxygen $1s$ state toward each of the protons which is evident in the figure. The figure also shows that, in the water molecule, the displacement of the $1s$ state leads to a net decrease of its amplitude on the nucleus. To quantify the impact of these core polarization effects on matrix elements describing transitions from the core to higher states, we have calculated the oxygen $1s$ contribution to the dipole moment of the water molecule, finding 0.0003 electron-bohr. As a point of reference, the net dipole moment which we compute for the entire molecule is 0.731 electron-bohr, in excellent agreement with the tabulated experimental value of 0.729 electron-bohr [30].

Turning now to the energies associated with these states, we note that although common approximations to density-functional theory give relatively poor results for the *absolute* positions of deep core levels, our results for the *shifts* in core-level energies show remarkable agreement with experiment. Accordingly, in comparing with experimental values, we maintain the relative placement of all of our eigenvalues (even between different molecules) by adding a single constant offset to our $1s$ eigen-energies. Figure 8 compares our multiresolution calculations of the energies of the oxygen $1s$ levels with the experimentally observed X-ray photo-emission spectrum of a mixture of water and molecular oxygen [29].

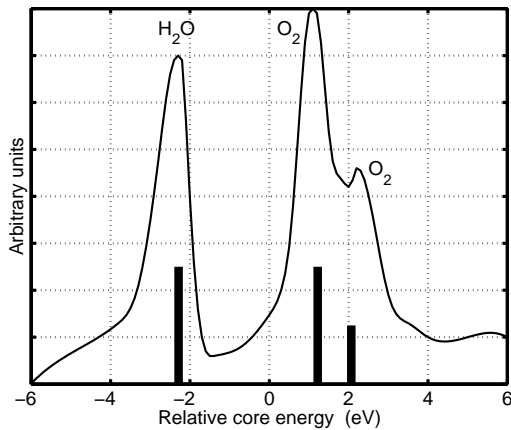


FIG. 8. Comparison of wavelet based all-electron calculation of the location of oxygen $1s$ states in the water and diatomic oxygen molecules (vertical bars) with experimental ESCA data (curve). Heights of bars for the O_2 molecule are in proportion to the multiplicity of the spin-state resulting from the photo-emission. The height of the bar for H_2O is arbitrary. ESCA data are after [29].

In molecular oxygen, the experiment shows significant splitting in the $1s$ levels, with noticeably different cross-sections for the two levels. This results from the propagation of paramagnetic bonding effects in the valence electrons down to the core levels. The stronger emission line results from the spin quartet state of the molecule (the result of photo-emission from the minority spin channel), which has twice the expected cross-section of the spin doublet state (the result of photo-emission from the majority spin channel). Our calculations, which treat the valence and core physics on a unified and equal footing, predict precisely this valence-core effect. The figure displays our results for the oxygen $1s$ Kohn-Sham eigenvalues (with a single, constant shift for both molecules) as vertical bars with heights proportional to the cross-sections expected for each spin channel. For the oxygen molecule, we find precisely the correct splitting and ordering for the two spin states. Finally, we note that our calculation of the relative positioning of the oxygen $1s$ state in the water molecule is also in excellent agreement with the experiment. (As the relative strengths of the spectral lines between oxygen and water depend upon the relative concentrations in the experiment, the height of the bar in the figure indicating our calculation of the water molecule is arbitrary.) With this level of agreement, such calculations can be a great aid in the interpretation of spectra of greater complexity.

VI. CONCLUSIONS

Multiresolution all-electron calculations allow the unified treatment of core and valence electrons where the local-density approximation is the sole approximation without systematic control. We have demonstrated that,

with this approach, study of the impact of valence behaviors on core electrons is straightforward and that meaningful core polarization effects and core-level shifts may be extracted to aid in the interpretation of experimental data such as ESCA.

Further, we have shown that, with the use of newly developed techniques, such calculations may be carried out with an effort comparable to the corresponding pseudopotential calculations, thereby establishing for the first time multiresolution analysis as a *viable* approach to all-electron calculations. By accounting in detail for the computational demands of our calculations, we have established a standard against which the performance of future wavelet calculations should be compared.

ACKNOWLEDGMENTS

This work supported by the US DOE ASCI ASAP Level 2 program (Contract No. B347887). TDE would like to thank the Research Council of Norway. Computational support provided by the Cornell Center for Materials Research.

-
- [1] M.C. Payne et al., *Rev. Mod. Phys.* **64**, 1045 (1992).
 - [2] David Feller and Ernest R. Davidson. *Basis Sets for Ab Initio Molecular Orbital Calculations and Intermolecular Interactions*, volume 1 of *Reviews in Computational Chemistry*. VCH, New York, 1990.
 - [3] O.K. Andersen, *Phys. Rev. B* **12**, 3060 (1975).
 - [4] D.J. Singh. *Planewaves, Pseudopotentials and the LAPW Method*. Kluwer Academic Publishers, Netherlands, 1994.
 - [5] E. Wimmer, H. Krakauer, M. Weinert, and A.J. Freeman, *Phys. Rev. B* **24**, 864 (1981).
 - [6] T.A.Arias et al. *Proceedings of the '94 Mardi Grad Conference: Toward Teraflop Computing and new Grand Challenge Applications*, edited by R.K. Kalia and P. Vashishta (Nova Science Publishers, Commack New York), p.23.
 - [7] T.A. Arias, *Rev. Mod. Phys.* **71**, 267 (1999).
 - [8] S. Han, K.J. Cho, and J. Ihm, *Phys. Rev. B*, **60**, 1437 (1999).
 - [9] K. Cho, T.A. Arias, J.D. Joannopoulos and Pui K. Lam, *Phys. Rev. Lett.* **71**, 1808 (1993).
 - [10] Siqing Wei and M.Y. Chou, *Phys. Rev. Lett.* **76**, 2650 (1996).
 - [11] C.J. Tymczak and X.-Q.Wang, *Phys. Rev. Lett.* **78**, 3654 (1997).
 - [12] O. Ivanov and V.P. Antropov, *J. Appl. Phys.* **85**, 4821 (1999).
 - [13] S.Goedecker and O.Ivanov, *Solid State Commun.* **105**, 65 (1998).
 - [14] S. Mallat, *Trans. Amer. Math. Soc.* **315**, 69 (1989).
 - [15] Y. Meyer. *Ondelettes, fonctions splines et analyses*

graduées. Lectures given at the University of Torino, Italy, 1986.

- [16] Y. Meyer. *Ondelettes et Opérateurs*. Herman, Paris, 1990.
- [17] Ross A. Lippert, T.A. Arias and Alan Edelman, *J. Comput. Phys.* **140**, 278 (1998).
- [18] Sohrab Ismail-Beigi and T.A. Arias, *Computer Physics Communications* **128**, 1 (2000).
- [19] T.A. Arias, M.C. Payne and J.D. Joannopoulos, *Physical Review Letters* **69**, 1077 (1992).
- [20] S. H. Vosko, L. Wilk, and M. Nusair, *Can. J. Phys.* **58**, 1200 (1980); S. H. Vosko and L. Wilk, *Phys. Rev. B* **22**, 3812 (1980).
- [21] M. Teter, *private communication*.
- [22] G.P.Lepage, “How to renormalize the Schroedinger Equation”, *Lectures at the VIII Jorge Andre Swieca Summer School*, Brazil (1997).
- [23] P. Pulay, *Mol. Phys.* **17**, 197 (1969).
- [24] J.P. Perdew and Y. Wang, *Phys. Rev. B* **45**, 13244 (1992).
- [25] A.M. Rappe, K.M. Rabe, E. Kaxiras, and J.D. Joannopoulos, *Phys. Rev. B*, **41**, 1227 (1990).
- [26] T.D.Engeness and T.A.Arias, “High-Performance Semi-cardinal Multiresolution Analysis Calculations,” *to be published*.
- [27] M. Frigo and S.G. Johnson, “FFTW: An Adaptive Software Architecture for the FFT,” *Proc. ICASSP 1998*, vol. 3, p. 1381. The software package is available at <http://www.fftw.org>
- [28] J. Silcox, *Current Opinion in Solid State and Materials Science* **3**, 336 (1998).
- [29] K.Siegbahn et al. *ESCA applied to free molecules* North-Holland Publishing company, Amsterdam-London, 1969.
- [30] *Handbook of Chemistry and Physics* 76th edition, edited by D.R. Lide and H.P.R. Frederikse (CRC Press, Boca Raton Florida), p. 9-44.

level	N_x	N_y	Δ_x	Δ_y
0	4	4	-	-
1	4	4	1	1
2	3	3	1	1

TABLE I. Numerical representation of restricted multiresolution analysis in Figure 1: dimension (N_x, N_y) and location relative to parent (Δ_x, Δ_y) of each refinement level.

σ (a.u.)	Q (a.u.)
$\frac{1}{8Z}$	+3.132576693428 Z
$\frac{1}{4\sqrt{2}Z}$	-2.683558382240 Z
$\frac{1}{4Z}$	+0.550981688812 Z

TABLE II. Widths σ and norms Q of the three Gaussian charge distributions $Q \exp(-r^2/(2\sigma^2))/(\sqrt{2\pi}\sigma)^3$ superimposed to represent a nucleus of charge Z . All quantities reported in atomic units.

level	N_x	N_y	N_z	Δ_x	Δ_y	Δ_z
0	36	36	36	-	-	-
1	36	36	36	9	9	9
2	36	36	36	9	9	9
3	36	36	36	9	9	9
4	36	36	36	9	9	9
5	36	36	36	9	9	9
6	48	48	48	6	6	6
7	48	48	48	12	12	12
8	72	72	72	6	6	6
9	72	72	72	18	18	18

TABLE III. Restriction employed for all-electron calculations of calcium: dimension (N_x, N_y, N_z) and location relative to parent ($\Delta_x, \Delta_y, \Delta_z$) of each refinement level.

level	N_x	N_y	N_z	Δ_x	Δ_y	Δ_z
0	28	24	24	-	-	-
1	30	24	24	6	6	6
2	34	24	24	6	6	6
3	44	24	24	6	6	6
4	60	24	24	7	6	6
5	24	24	24	6	6	6
6	32	32	32	4	4	4
5	24	24	24	42	6	6
6	32	32	32	4	4	4

TABLE IV. Restrictions employed for all-electron calculation of oxygen molecule: dimension (N_x, N_y, N_z) and origin relative to its parent ($\Delta_x, \Delta_y, \Delta_z$) of each refinement level.

level	N_x	N_y	N_z	Δ_x	Δ_y	Δ_z
0	48	48	48	-	-	-
1	48	48	48	12	12	12
2	48	48	48	12	12	12
3	72	72	48	6	6	12
4	72	72	48	18	18	12
5	72	72	48	18	18	12
6	72	72	48	18	18	12

TABLE V. Restrictions employed for all-electron calculation of water molecule: dimension (N_x, N_y, N_z) and origin relative to its parent ($\Delta_x, \Delta_y, \Delta_z$) of each refinement level.

Quantity	MRA	V_{ps}
N_B	200,000	160,000
$N_{F/B}$	250	1600
$N_{F/T}$	$200 \cdot 10^6$	$180 \cdot 10^6$
N_A	32,000	8,500
T	8.2 hrs	3.4 hrs

TABLE VI. Analysis and comparison of computational demands of multiresolution analysis all-electron calculation (MRA) and plane-wave pseudopotential calculation (V_{ps}) of oxygen molecule within LSDA for basis sets reaching a similar level of convergence.